

Article

Triaxial Compression Strength Prediction of Fissured Rocks in Deep-Buried Coal Mines Based on an Improved Back Propagation Neural Network Model

Yiyang Wang^{1,2}, Bin Tang^{1,2,*}, Wenbin Tao³, Anying Yuan², Tianguo Li¹, Zhenyu Liu¹, Fenglin Zhang¹ and An Mao¹

¹ State Key Laboratory of Mining Response and Disaster Prevention and Control in Deep Coal Mines, Anhui University of Science and Technology, 168 Taifeng St., Huainan 232001, China; w960920yy@163.com (Y.W.); ltg0403@163.com (T.L.)

² School of Civil Engineering and Architecture, Anhui University of Science and Technology, 168 Taifeng St., Huainan 232001, China; ayyuan@aust.edu.cn

³ Anhui Transport Consulting and Design Institute, Hefei 230088, China; taowenbin0963@sina.com

* Correspondence: tangbin0554@163.com

Abstract: In deep coal mine strata, characterized by high ground stress and extensive fracturing, predicting the strength of fractured rock masses is crucial for stability analysis of the surrounding rock in coal mine strata. In this study, rock samples were obtained from construction sites in deep coal mine strata and intact, as well as fissured, rock specimens were prepared and subjected to triaxial compression tests. A numerical model based on the discrete element method was then established and the micro-parameters were calibrated. A total of 288 triaxial compression tests on the rock specimens under different conditions of confining pressure, loading rate, fissure dip angle, and fissure length, were conducted to obtain the triaxial compressive strength of the fractured rock specimens under different conditions. To address the limitations of traditional back propagation (BP) neural networks in solving stochastic problems, a modified BP neural network model was developed using a random factor and an interlayer mean square error corrected network model evaluation function. The traditional and modified BP neural network models were then employed to predict the triaxial compressive strength of the fractured rock specimens. Through comparative analysis, it was found that the modified BP neural network prediction model exhibited smaller errors and significantly reduced overfitting, making it an effective tool for predicting the strength of fractured rocks in deep coal mine strata.

Keywords: fissured rock specimen; triaxial compression tests; numerical tests; improved BP neural network prediction model



Citation: Wang, Y.; Tang, B.; Tao, W.; Yuan, A.; Li, T.; Liu, Z.; Zhang, F.; Mao, A. Triaxial Compression Strength Prediction of Fissured Rocks in Deep-Buried Coal Mines Based on an Improved Back Propagation Neural Network Model. *Processes* **2023**, *11*, 2414. <https://doi.org/10.3390/pr11082414>

Academic Editors: Hong Wong, Dan Ma, Lang Liu, Jiangyu Wu and Wen Zhong

Received: 25 July 2023

Revised: 5 August 2023

Accepted: 8 August 2023

Published: 10 August 2023



Copyright: © 2023 by the authors. Licensee MDPI, Basel, Switzerland. This article is an open access article distributed under the terms and conditions of the Creative Commons Attribution (CC BY) license (<https://creativecommons.org/licenses/by/4.0/>).

1. Introduction

As China's shallow coal resources have nearly been exhausted, coal mining in China has shifted to deep-seated strata. Deep-seated strata are characterized by high ground stress and well-developed discontinuities, such as joints and fractures, which result in engineering disasters, such as roof collapse and significant deformation of the surrounding rock, posing significant risks to coal mining operations. The presence of fractures in deep-seated strata rock masses has a substantial contribution on the mechanical character of rocks. Accordingly, the mechanical properties of rock masses containing fractures under the conditions of high ground stress in deep-seated coal strata become a key issue in evaluating the stability of the surrounding rock and in supporting the surrounding rock in coal mining operations.

Many researchers have conducted experimental tests on rock specimens, which contain fissures or joints. Wang researched the failure behaviors and mechanical properties of soft rocks containing different fissures under uniaxial compression. The influence of the

fissure dip angle, fissure length, and fissure number on the strength of the rock specimens were studied [1]. Liu studied the strain and stress distribution characteristics of rock specimens containing a single pre-existing fissure under uniaxial compression [2]. Tan carried out uniaxial compressive tests on cubic rock-like specimens with fissures, and the effects of the fissure number on the mechanical properties were studied [3]. In deep-buried strata, rock masses are commonly damaged under triaxial compressive conditions. Therefore, some researchers have studied the mechanical behaviors of fissured rocks under triaxial compression. Yang conducted triaxial compressive tests on both intact and fissured sandstone specimens. Stress–strain curves for sandstone specimens containing different fissures were obtained. The crack evolution characteristics were also studied by using the acoustic emission technique [4]. Li studied the failure mechanism of rock with prefabricated cracks by conducting compression failure tests on rock with prefabricated fractures under different true triaxial conditions [5]. Zhou conducted the true triaxial compressive tests on coarse and fine sandstone specimens containing two parallel fissures, and the failure characteristics were studied [6]. Liu conducted triaxial pulling tests on sandstone rock specimens, which contained a single fissure, and studied the influence of the fissure parameters on the strength of the specimens [7]. Although experimental tests on fissured rocks can provide accurate data, the lengthy preparation time and high cost of experimental tests make it difficult to obtain large quantities of data for research and analysis purposes.

Different experimental tests on rock specimens containing fissures have been conducted and the mechanical parameters, as well as the failure behaviors, of fissured rocks have been analyzed. Nevertheless, some drawbacks have been encountered during the implementation of experimental tests. For example, only the stress and strain distribution and evolution behaviors on the surface of rock specimens can be measured. Moreover, the failure processes of rock specimens cannot be clearly observed in experimental tests. Therefore, numerical tests on fissured rock specimens have been conducted by researchers. Zare conducted numerical tests on rock-like specimens containing fissures and compared them with experimental tests [8]. Zhao established particle flow models of rock samples with flaws and conducted numerical tests [9]. The influence of the inclination angle on the mechanical properties and crack propagation behaviors of the specimens were examined. Manouchehrian carried out numerical tests on rock specimens with notches under triaxial compression to investigate the influence of the notch length on the fracturing behavior of the specimen. Wang studied the mechanical behaviors of sandstone containing a single open fissure under uniaxial compression by conducting numerical tests [10]. Feng investigated the influence of two unparallel fissures on the mechanical behavior of rock-like specimens subjected to uniaxial compression through numerical tests [11]. Wang studied crack coalescence modes and micro-crack propagation law of fissured sandstone specimens by conducting numerical uniaxial tests [12]. Chen established a discrete element model of rock specimens containing X-shaped fissures and conducted uniaxial compressive tests. The influence of fissures on the mechanical properties of rock specimens were investigated [13].

Numerical tests on fissured rocks provide a more efficient and cost-effective approach to obtain the mechanical properties of fractured rock masses under different conditions [14,15]. However, there are numerous factors that influence the strength of fractured rocks, making it difficult to analyze experimental results through traditional fitting methods. Therefore, some researchers have introduced machine learning techniques to analyze the outcomes of rock experiments. Yu predicted the uniaxial compressive strength of rock by using swarm intelligence optimization algorithms [16]. Ren established the back propagation (BP) neural network and applied it in rock micro-parameter calibration of PFC numerical models [17]. Zhang applied the BP neural network model to predict the rock parameters in underground coal mines [18]. BP neural networks have found extensive applications in the domain of rock mechanics due to their strong learning capability, robustness, ability to achieve parallel processing through distributed computing, and high computational efficiency. However, they still have certain limitations when it comes to analyzing problems with randomness. In particular, the choice of evaluation metrics significantly influences the

performance of the network, potentially leading to overfitting and substantial errors in the output predictions of the BP model.

In order to investigate the mechanical properties of deep-seated fissured rock masses in coal mines, this study first conducted triaxial compression laboratory tests on intact and fractured rock specimens. Based on the test results, a numerical model was developed utilizing the discrete element method, with the calibration of micro-mechanical parameters. After the numerical tests were verified by experimental tests, 288 triaxial compression numerical tests on rock specimens under different confining pressures, loading rates, fissure dip angles, and fissure lengths were then conducted to obtain the triaxial compression strength of the rock specimens subjected to various conditions. To address the limitations of conventional back propagation (BP) neural networks in dealing with randomness, an improved BP neural network model was developed for predicting the triaxial compressive strength of fissured rock. The model utilized random factors and interlayer mean square error correction as the evaluation function. The triaxial compressive strength of fractured rock was predicted using both the conventional and improved BP neural network models. Through comparative analysis, it was found that the modified BP neural network model had smaller prediction errors and significantly reduced overfitting, making it an effective tool for predicting the strength of fractured rock in deep-seated geological formations in coal mines.

2. Experimental Tests on Fissured Rock Specimens

2.1. Test Specimen Preparation

The rock samples were collected from deep-buried sandstone strata from coal mines in Huainan coal field, China. The rock samples were processed into standard cylindrical specimens, with a diameter of 50 mm and a height of 100 mm, according to ISRM's suggestions [19]. In order to investigate the mechanical properties of fractured rocks under triaxial compression conditions, fissured rock specimens were fabricated. The fissures were cut at the center of the processed rock specimens, with a length of 20 mm and a width of 1 mm. The fissure dip angles were assigned values of 0° , 15° , 30° , 45° , 60° , and 90° , as depicted in Figure 1.

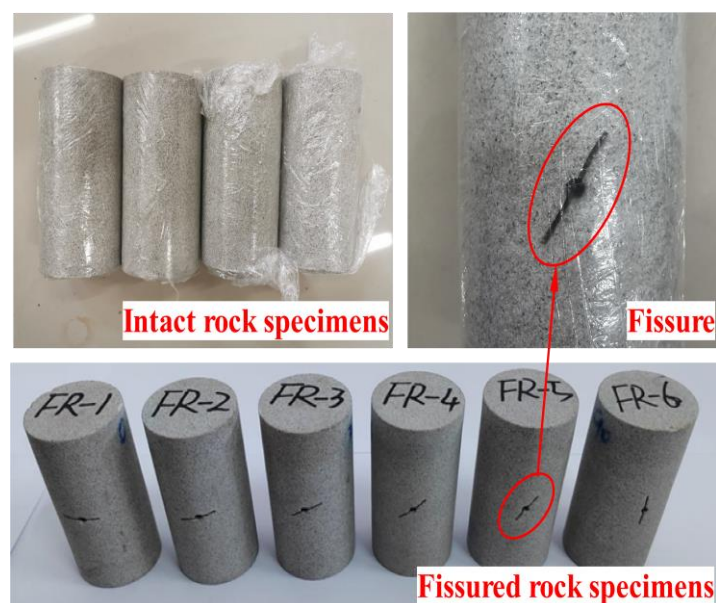


Figure 1. Fissured rock specimens.

2.2. Test Apparatus and Procedures

The experiments were carried out utilizing a ROCK 600-50HT rock mechanics testing system manufactured by TOP INDUSTRIE from France, as illustrated in Figure 2. The

ROCK 600-50HT testing system comprises a control system, triaxial chamber, servo loading system, and data acquisition system. The system has a maximum axial loading capacity of 1000 kN, a maximum confining pressure of 60 MPa, and a maximum displacement capacity of 25 mm.

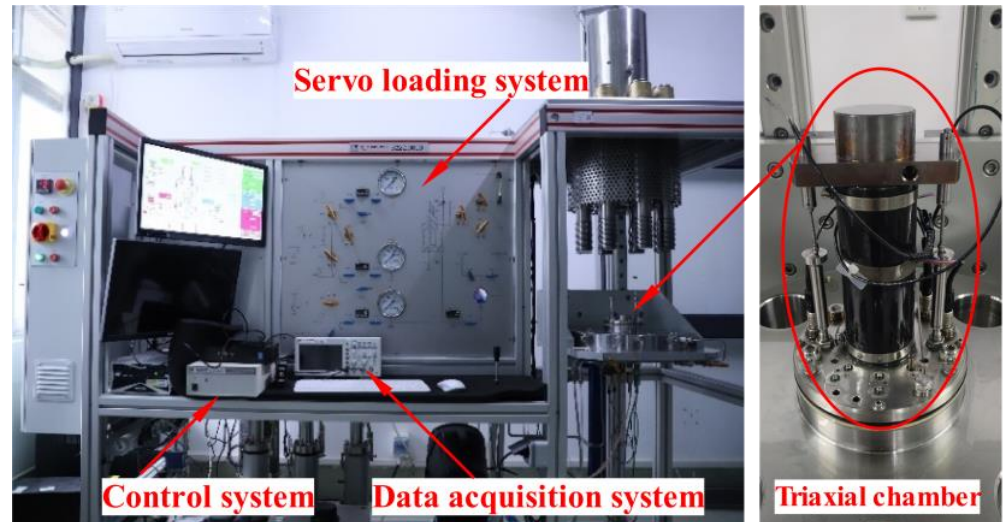


Figure 2. ROCK 600-50HT rock mechanics testing system.

In order to study the mechanical behavior of the Huainan sandstone specimens, which contain fissures, under various fissure dip angles, confining pressures, and loading rates, orthogonal tests were designed and implemented. Firstly, the specimens were placed within the triaxial chamber and the axial, as well as the confining pressures, were increased to the expected level, with a rate of 0.05 MPa/s, simultaneously. Subsequently, the specimens were loaded under different loading rates and confining pressures until the failure of the specimens. The test parameters are shown in Table 1.

Table 1. Parameters of the triaxial test.

Specimen Number	Fissure Dip Angle (°)	Fissure Length (mm)	Loading Rate (mm/s)	Confining Pressure (MPa)
IR-15	N/A	N/A	0.001	15
IR-20	N/A	N/A	0.001	20
IR-25	N/A	N/A	0.001	25
IR-30	N/A	N/A	0.001	30
FR-1	0	20	0.003	15
FR-2	15	20	0.001	20
FR-3	30	20	0.003	25
FR-4	45	20	0.001	30
FR-5	60	20	0.003	15
FR-6	90	20	0.001	20

2.3. Test Results

Figure 3 illustrates the stress–strain curves for the fissured specimens. The stress and strain values have near linear relations at the beginning stage of the tests. Subsequently, the stress–strain curves for the specimens experienced fluctuations before reaching the peak stress. This phenomenon could be caused by crack mobilization. The stress–strain curves turned from approximate straight lines to curves when approaching the peak stress. As shown in Figure 3, it can be noted that at a confining pressure of 30 MPa, the rock specimens begin to exhibit significant ductility. The peak stress values of the fissured specimens are shown in Table 2. The decrease in the peak stress tends to increase and then decrease with

the increase in the dip angles in the fissures. The impact of fissures on the mechanical properties of rocks is most pronounced at a dip angle of 45° .

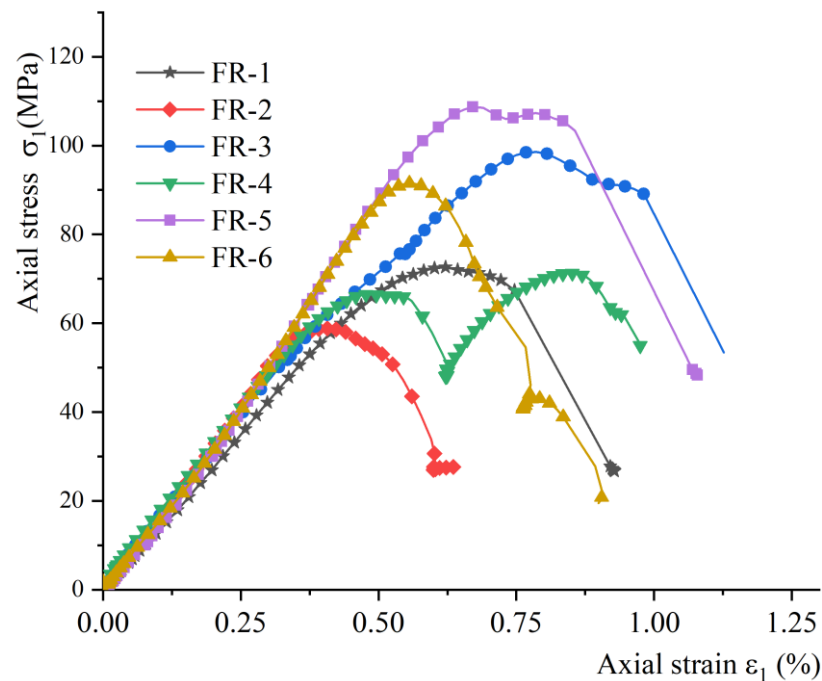


Figure 3. Stress–strain curves of the fissured specimens.

Table 2. Test results for the fissured specimens.

Specimen Number	Fissure Dip Angle ($^\circ$)	Fissure Length (mm)	Loading Rate (mm/s)	Confining Pressure (MPa)	Peak Stress σ_c (MPa)
FR-1	0	20	0.003	15	76.21
FR-2	15	20	0.001	20	58.86
FR-3	30	20	0.003	25	98.56
FR-4	45	20	0.001	30	54.56
FR-5	60	20	0.003	15	107.31
FR-6	90	20	0.001	20	91.54

3. Numerical Tests on Fissured Rock Specimens

The triaxial compressive strength of fractured rock specimens is affected by various factors, and the extensive range of combinations of these factors poses challenges, namely in conducting separate experimental tests for every scenario. For the purpose of studying the influence of various parameters (confining pressure, prefabricated fissure angles, etc.) on the specimen's mechanical character, more tests under different parameters need to be conducted. Considering experimental tests are time consuming and costly, numerical tests were implemented. First of all, discrete element method (DEM) numerical models of the specimens were established by using particle flow code (PFC) simulation. Secondly, numerical tests were performed, and the obtained results were compared with those from the experimental tests, enabling the calibration of micro-parameters for the DEM models. Subsequently, the accuracy of the numerical tests was validated through a comparative analysis of the experimental and numerical test results for the fissured specimens. Finally, more numerical tests with various parameters were conducted and the test results were recorded.

3.1. Numerical Model Establishment

A model of an intact cylinder specimen, with a height of 100 mm and a diameter of 50 mm, was developed. The model contained 44,143 particles with diameters ranging from 0.7 to 1.1 mm. A cylindrical wall and two panel walls were built to apply the confining load and axial load, respectively (shown in Figure 4).

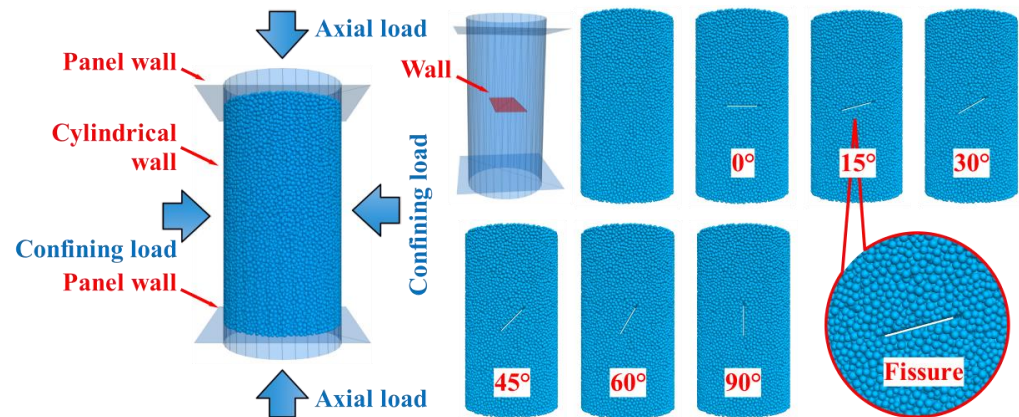


Figure 4. The PFC numerical model of the fissured rock specimens.

Traditionally, the method of removing particles has been used to form fissures in PFC models. However, deleting particles can result in uneven fissure surfaces, which is inconsistent with reality. As shown in Figure 4, in this study, during the numerical model pre-pressing phase, a wall is created at the joint position through editing the FISH code, and prefabricated fissures are generated within the wall after the pre-pressing is completed. The fissure surfaces generated using this method are smooth and unaffected by the particle radius. Using the aforementioned method, a PFC numerical model of the fissured rock specimens is established, with the actual rock specimen parameters, where the fissure length is set to 20 mm, and the fissure dip angle is set to 0°, 15°, 30°, 45°, 60°, and 90°.

3.2. Parameter Calibrations for the Numerical Model

In order to calibrate the micro-parameters of the PFC numerical model, laboratory triaxial compression tests were conducted on four intact specimens, along with corresponding numerical simulations. The numerical tests were repeated multiple times until the mechanical behavior of the numerical model closely matched that of the rock specimens. As demonstrated in Table 3, the errors in the triaxial compressive strength between the numerical model and the rock specimens were less than 5%, thus validating the accuracy of the numerical experiments. The calibrated micro-parameters of the PFC model are shown in Table 4.

Table 3. Comparison of the triaxial compression strength between the experimental and numerical tests.

Specimen Number	Confining Pressure (MPa)	Triaxial Compression Strength (MPa)		Error (%)
		Experimental Tests	Numerical Test	
IR-1	15	82.40	84.56	15
IR-2	20	99.01	103.43	20
IR-3	25	118.27	123.35	25
IR-4	30	132.74	136.74	30

Table 4. Micro-parameters of the numerical model.

Parameters	Value
Effective modulus (GPa)	18.51
Stiffness ratio	2.42
Parallel bonding effective modulus (Gpa)	18.51
Parallel bonding stiffness ratio (GPa)	2.42
Tensile strength (MPa)	104.38
Bonding strength (MPa)	43.49
Parallel bonding friction angle (°)	47

3.3. Numerical Test Results

Upon calibrating the micro-parameters of the numerical model, to further substantiate the precision of the numerical experiments, numerical models of the fissured rock specimens were developed employing the parameters derived from the aforementioned rock specimens. The procedures for the numerical tests were established by referring to the experimental tests, thereby simulating the experimental tests conducted on the fissured rock specimens. By comparing the results of the experimental tests with the numerical tests, the accuracy and effectiveness of the numerical tests were further validated.

Numerical tests were conducted encompassing all combinations of the test parameters, including four confining pressures (15 MPa, 20 MPa, 25 MPa, 30 MPa), six fracture angles (0° , 15° , 30° , 45° , 60° , 90°), four fracture lengths (10 mm, 15 mm, 20 mm, 25 mm), and three loading rates (0.001 mm/s, 0.002 mm/s, 0.003 mm/s). A total of 288 numerical triaxial compression tests were conducted on the fissured rock specimens, and the triaxial compressive strength values were obtained. Due to space constraints, only a portion of the test results are shown in Figure 5 and Table 5. Figure 5a presents the stress–strain curve obtained from the numerical experiments under a confining pressure of 20 MPa and a fissure length of 20 mm. It can be observed that the specimen exhibits the lowest strength when the fissure dip angle is 45° . Figure 5b illustrates the failure characteristics of different fissured specimens in the numerical experiments, where the blue dots represent cracks. As the load increases, the cracks always initiate at the fissure tip and then propagate along the diagonal direction, eventually leading to specimen failure.

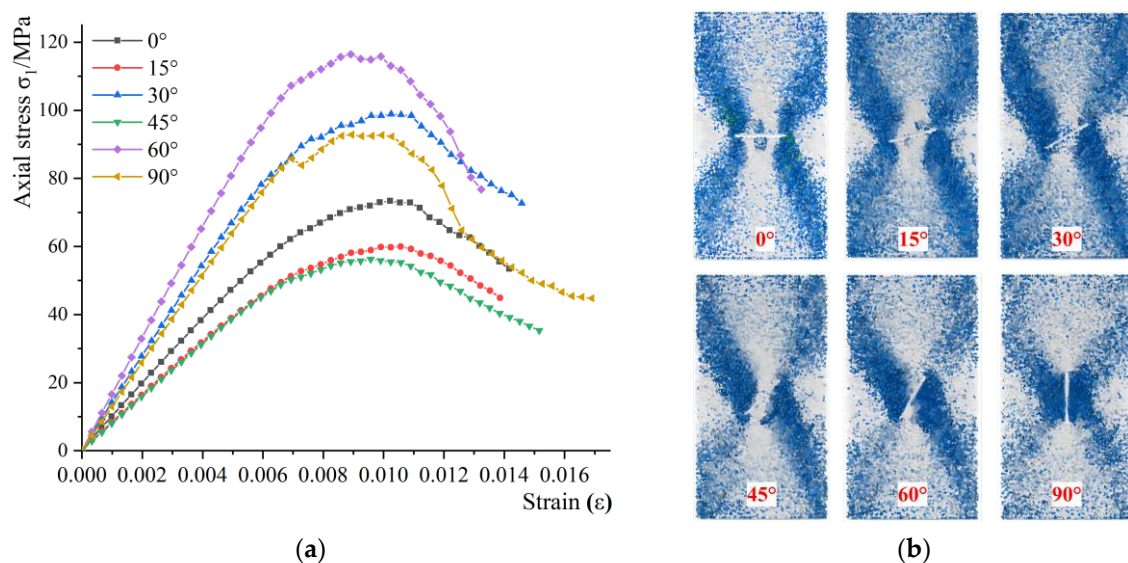


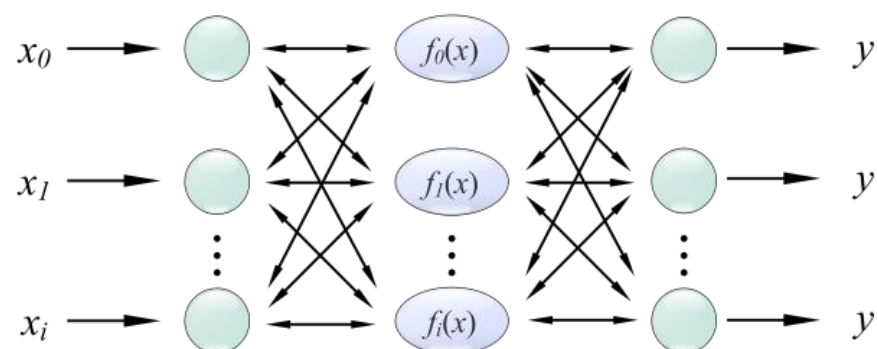
Figure 5. Partial numerical test results for the fissured rock specimens (20 MPa confining pressure and 20 mm fissure length): (a) stress–strain curves for the numerical tests; (b) failure characteristics of the fissured specimens.

Table 5. Numerical test results for the partial fissured rock specimens under triaxial compression.

Number	Fissure Length (mm)	Fissure Dip Angle ($^{\circ}$)	Confining Pressure (MPa)	Loading Rate (mm/s)	Strength (MPa)
1	10	0	15	0.001	83.58
2	10	15	15	0.001	82.75
3	10	30	15	0.001	83.24
4	10	45	15	0.001	87.44
5	10	60	15	0.001	79.86
6	10	90	15	0.001	74.79
7	10	0	20	0.001	75.94
8	10	15	20	0.001	74.82
9	10	30	20	0.001	75.31
10	10	45	20	0.001	77.70
...
284	25	15	30	0.003	60.68
285	25	30	30	0.003	60.89
286	25	45	30	0.003	61.10
287	25	60	30	0.003	61.31
288	25	90	30	0.003	64.91

4. Rock Strength Prediction Model Based on Artificial Neural Networks

The strength of fissured rock specimens is influenced by many factors, such as the confining pressure, fissure dip angle, fissure length, fissure opening, etc. Therefore, it is difficult to establish a strength prediction model for fissured rocks using conventional analytical models. A back propagation (BP) neural network is a multi-layer feed-forward network trained according to error back propagation, the basic idea is the gradient descent method, using the gradient search technique, to minimize the actual output value of the network and the expected output value of the error mean square difference [20]. As shown in Figure 6, the computational procedure of a BP neural network involves a forward propagation stage and a backward propagation stage. During the forward propagation stage, the input pattern is sequentially processed through the input layer, hidden layer, and output layer. The state of each neuron in a layer only influences the state of the subsequent layer. If the desired output is not achieved at the output layer, the backward propagation stage is triggered. Here, the error signal travels back through the original connection pathway, and the weight of each neuron is adjusted to minimize the error signal.

**Figure 6.** The BP neural network training graph.

4.1. The Algorithm Steps in the BP Neural Network

The back propagation (BP) neural network is a type of multi-layer feed-forward network that is trained using the error back-propagation algorithm. It is based on the concept of gradient descent, wherein the network's actual output values are adjusted using a gradient search technique to minimize the mean squared difference between the actual and expected output values [21].

The procedure for the BP neural network algorithm is outlined below [21]:

Step1: Weight Initialization.

$$w_{sq} = \text{Random}(\cdot) \quad (1)$$

where sq denotes ij, jk , and w represents the corresponding node connection weight.

Step 2: Input the P learning samples sequentially, with the current input being p samples.

Step 3: Calculate the outputs of each layer sequentially.

$$x'_j, y_k, j = 0, 1, \dots, n_1, k = 0, 1, \dots, m - 1 \quad (2)$$

Step 4: Calculate the back propagation error.

$$\delta_{jk}^{(p)} = (d_k^{(p)} - y_k^{(p)})y_k^{(p)}(1 - y_k^{(p)}) \quad (3)$$

where $k = 0, 1, 2, \dots, m - 1$;

$$\delta_{ij}^{(p)} = \sum_{k=0}^{n_2} (\delta_{jk}^{(p)} w'_{jk} x'_j{}^{(p)} (1 - x'_j{}^{(p)})) \quad (4)$$

where $j = 0, 1, 2, \dots, n_1$.

Step 5: Record the number of samples already learned, p . If p is less than P , go back to step 2 and continue the computation. If p equals P , proceed to step 6.

Step 6: Update the weights and thresholds for each layer according to the weight adjustment formula.

Step 7: Recalculate x'_j, y_k , and the total error E_A using the updated weights. If the conditions $|d_k^{(p)} - y_k^{(p)}| < \varepsilon$ (or $E_A < \varepsilon$) are satisfied for each p and k , or the maximum number of learning iterations is reached, the learning process is terminated. Otherwise, go back to step 2 and continue with a new round of learning.

4.2. Stochastic Improvement of BP Neural Networks

The back propagation (BP) neural network, widely utilized in machine learning, boasts numerous advantages. However, it is not exempt from a common limitation known as overfitting. Overfitting arises when a model excessively adapts to the training data, resulting in poor generalization capabilities on unseen data. To tackle this issue, regularization methods have been introduced to effectively control the magnitudes of network weights. These methods involve modifying the error function by incorporating a regularization term that imposes constraints beyond the sample data. In the case of neural networks, the mean squared error (MSE) function is commonly employed to appraise training effectiveness. It is defined as follows:

$$mse = \frac{1}{P} \sum_{n=1}^P (d^{(p)} - y^{(p)})^2 \quad (5)$$

where $d^{(p)}$ and $y^{(p)}$ represent the target value and prediction value for the i -th training sample among P training samples, respectively. In the regularization method, the network performance function $msereg$ is modified as follows:

$$msereg = \gamma mse + (1 - \gamma) msw \quad (6)$$

$$msw = \frac{1}{N} \sum_{i=1}^N w_j^2 \quad (7)$$

where γ represents the proportion coefficient and msw denotes the mean square weight.

By adopting a new performance index function it is ensured that the network has smaller weights, while minimizing the training error. This effectively results in the auto-

matic reduction of the network's size, which in turn reduces the chances of overfitting. Overfitting occurs when the dimension of the network is considerably smaller than the magnitude of the training dataset. This is beneficial for enhancing the network's generalization ability. The improved algorithm workflow is described in Figure 7.

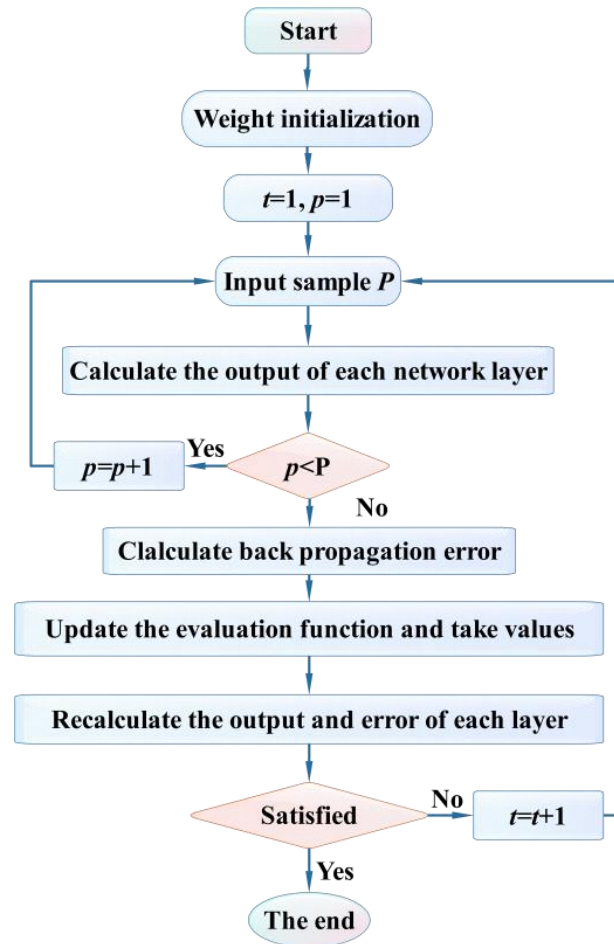


Figure 7. Improved BP network algorithm flow chart.

4.3. Stochastic Prediction Model for Fissured Rock Specimen Strength

In order to enhance the precision of the stochastic prediction model for the strength of fissured rock samples, the confining pressure, fissure length, and fissure dip angle were used as inputs into the improved BP neural network stochastic prediction model. The compressive strength is taken as the output of the stochastic prediction model.

In addition to the input and output layers, the determination of the hidden layers also relates to the prediction efficiency and the accuracy of the results of the network model. Usually, in order to ensure the efficiency and accuracy of the network model, Equation (8) is used to calculate the number of intermediate layer cells, according to the principle of model lightweighting.

$$T = \sqrt{AB + 1.68B + 0.93} \quad (8)$$

where T is the ideal number of neural units in the intermediate layer, and A and B represent the count of the input and output parameters utilized in the network model, respectively.

Substituting the number of model input and output parameters into Equation (8), results in:

$$T = \sqrt{3 \times 1 + 1.68 \times 1 + 0.93} \quad (9)$$

$$T = \sqrt{5.61} \approx 2.37 \quad (10)$$

Consequently, the hidden layer in the improved BP neural network-based stochastic prediction model can be determined to comprise three cells through the calculation.

4.4. Application of Fissured Rock Specimen Strength Prediction

Before establishing the model, it is necessary to pre-divide the dataset into a training set and a testing set. The training set is used for model training, while the testing set is used to verify and evaluate the reliability and generalization performance of the trained model. Proper dataset partitioning has a significant impact on the final generalization performance of the model. When the proportion of the training set is too high and the proportion of the testing set is relatively low, it can lead to overfitting, where the model performs well on the training set but poorly on the testing set. Conversely, when the proportion of the training set is too low and the proportion of the testing set is too high, it can lead to underfitting, where the model performs poorly on both the training set and the testing set [22]. In BP neural network model training, it is common to divide the dataset into a ratio of 7:3 or 8:2 for training and testing purposes [23]. Therefore, 75% of the data was chosen as the training set, while the remaining 25% of the data was used as the testing set. The training set consisted of 216 data points, while the testing set contained 72 data points.

To evaluate the predictive performance of the conventional BP neural network and the improved BP neural network model, the determination coefficient (R^2), root mean square error (RMSE), and mean absolute percentage error (MAPE) are used as evaluation metrics to measure the model's generalization ability. The corresponding calculation formulas are illustrated in Table 6. R^2 represents the precision of the model in fitting the data, and a value closer to 1 indicates a better fit. The RMSE reflects the deviation between the predicted values and the actual values, while the MAPE represents the average absolute error between the predicted values and the actual values. Smaller values for both metrics indicate better generalization performance of the model.

Table 6. Evaluation index for the prediction model.

Evaluation Index	Calculation Formula	Evaluation Criteria
Determination coefficient (R^2)	$R^2 = 1 - \frac{\sum_{i=1}^n (y_i - \hat{y}_i)^2}{\sum_{i=1}^n (y_i - \bar{y}_i)^2}$	The larger the R^2 value, the better the performance of the model.
Root mean square error (RMSE)	$RMSE = \sqrt{\frac{1}{n} \times \sum_{i=1}^n (y_i - \hat{y}_i)^2}$	The smaller the RMSE value, the better the performance of the model.
Mean absolute percentage error (MAPE)	$MAPE = \sum_{i=1}^n \left \frac{y_i - \hat{y}_i}{y_i} \right \times \frac{100\%}{n}$	The smaller the MAPE value, the better the performance of the model.

Figure 8 presents the comparison results for the predicted values and measured values between the two models, namely the conventional BP neural network and the improved BP neural network. As shown in Figure 8, the blue and orange scattered points represent the predicted results of the models for the samples in the training set and the testing set, respectively. The former reflects the learning ability of the models for complex nonlinear relationships in known data, while the latter reflects the generalization ability of the models for predicting unknown data. From Figure 8, it can be observed that the scattered points for the improved BP neural network model are more concentrated near the reference line compared to the conventional BP neural network model, indicating that the improved BP neural network model achieves better prediction results for the triaxial compressive strength of fractured rock specimens. The R^2 , RMSE, and MAPE for the improved BP neural network model using the training set are 0.992, 3.53, and 4.91%, respectively, which are better than those of the conventional BP neural network model (0.965, 5.42, and 7.89%). Moreover, the R^2 , RMSE, and MAPE for the improved BP neural network model using the testing set are 0.985, 6.29, and 9.83%, respectively, outperforming the conventional BP

neural network model (0.961, 10.35, and 14.72%). Based on the values of the evaluation metrics, it can be concluded that the improved BP neural network model exhibits better performance using both the training and testing datasets compared to the conventional BP neural network model.

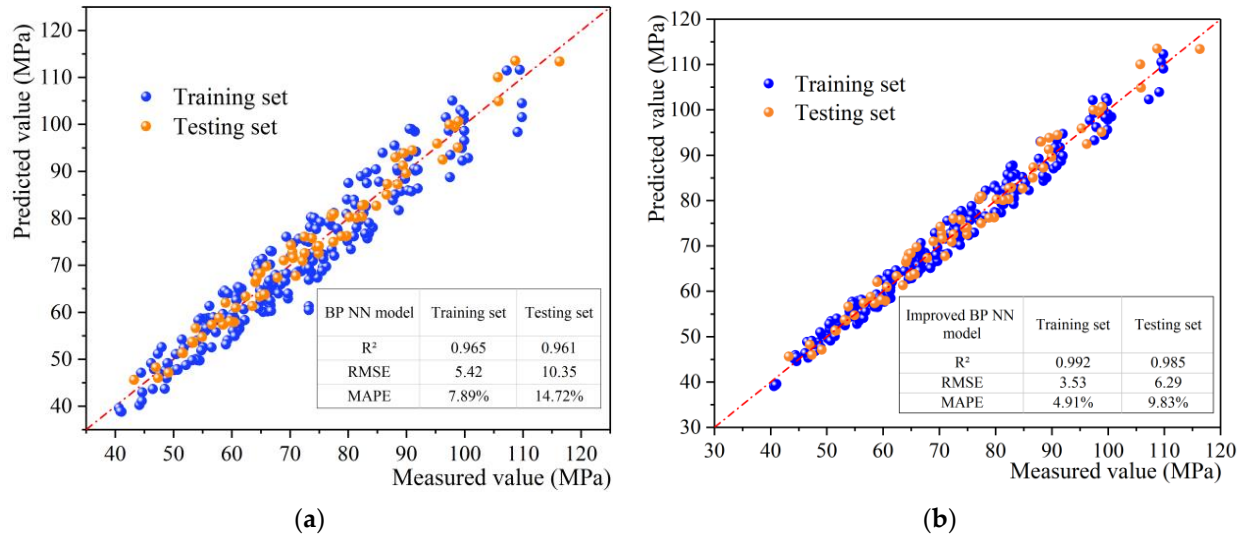


Figure 8. Comparison between the predicted values and measured values under the conventional and improved BP neural network model: (a) conventional BP neural network model; (b) improved BP neural network model.

5. Conclusions

The experimental and numerical triaxial compression tests on fissured rock specimens containing pre-existing fissures were conducted and the improved BP neural network model was established for strength prediction of fissured rock specimens under triaxial compression. Some conclusions can be made, as follows:

1. Triaxial compression tests were conducted on intact and fissured rock specimens under different confining pressures, fracture angles, and loading rates to obtain the triaxial compression strength of the fissured rock specimens under different conditions, serving as reference data for the numerical experiments.
2. Discrete element method numerical models were established for the intact and fissured rock specimens. After calibrating the micro-parameters of the numerical models, numerical triaxial compression tests were conducted on the rock specimens and validated through experimental tests. The error in the numerical experiments was within 5%, indicating a high level of accuracy of the numerical models.
3. Numerical triaxial compression tests on the fractured rock specimens were conducted under four confining pressures, four fracture lengths, six fracture inclinations, and three loading rates, resulting in a total of 288 sets of triaxial compression test data for the fractured rock specimens. These data were used to train a predictive model on the triaxial compressive strength of fractured rock. By employing a modified back propagation neural network based on random factor and interlayer mean square error correction, the predictive model for the triaxial compressive strength of fractured rock was established. The R^2 , RMSE, and MAPE for the improved BP neural network model in the training set was 0.992, 3.53, and 4.91%, respectively, indicating that the model's prediction performance is superior to that of the traditional BP neural network model.

In summary, this study combines machine learning with rock mechanics to achieve intelligent prediction of rock strength using a limited number of rock mechanics tests. Compared to traditional experimental methods, this approach saves a significant amount of manpower, financial resources, and time, providing a new reference for predicting the

strength of fractured rocks under high stress conditions in deep coal mine strata. However, the training process for the BP neural network requires iterative computations through the back propagation algorithm to adjust the network's weights and biases. As a result, the training speed is relatively slow. In the future, the authors will continue to conduct further research on accelerating the training speed of BP neural networks.

Author Contributions: Conceptualization, B.T. and W.T.; methodology, B.T. and Y.W.; software, Y.W. and A.Y.; validation, Y.W., T.L. and Z.L.; formal analysis, F.Z.; investigation, A.M.; resources, Y.W.; data curation, Y.W.; writing—original draft preparation, Y.W.; writing—review and editing, B.T.; visualization, W.T.; supervision, B.T.; project administration, B.T.; funding acquisition, B.T. and W.T. All authors have read and agreed to the published version of the manuscript.

Funding: This research was funded by the Natural Science Foundation of Anhui Province, China, grant number 2208085ME118; the Natural Science Foundation of the Education Department of Anhui Province, grant number KJ2021ZD0049; and the Fund of the State Key Laboratory of Mining Response and Disaster Prevention and Control in Deep Coal Mines, grant number SKLMRDPC21KF13 and SKLMRDPC20ZZ04. The APC was funded by the Natural Science Foundation of Anhui Province, China.

Data Availability Statement: Some or all of the data, models, or code that support the findings in this study are available from the corresponding author upon reasonable request.

Conflicts of Interest: The authors declare no conflict of interest.

References

1. Wang, Y.; Tang, J.; Dai, Z.; Yi, T. Experimental study on mechanical properties and failure modes of low-strength rock samples containing different fissures under uniaxial compression. *Eng. Fract. Mech.* **2018**, *197*, 1–12. [[CrossRef](#)]
2. Liu, L.; Liu, Y.; Li, H.; Wu, X.L.A.R. Full-field strain evolution and characteristic stress levels of rocks containing a single pre-existing flaw under uniaxial compression. *Bull. Eng. Geol. Environ.* **2020**, *79*, 3145–33161. [[CrossRef](#)]
3. Tan, Y.; Guo, W.; Zhao, T.; Yu, F.; Huang, B.; Huang, D. Influence of fissure number on the mechanical properties of layer-crack rock models under uniaxial compression. *Adv. Civ. Eng.* **2018**, *2018*, 7179831. [[CrossRef](#)]
4. Yang, S.; Huang, Y.; Ranjith, P. Failure mechanical and acoustic behavior of brine saturated-sandstone containing two pre-existing flaws under different confining pressures. *Eng. Fract. Mech.* **2018**, *193*, 108–121. [[CrossRef](#)]
5. Li, Z.; Wang, L.; Li, W. Mechanical Behavior and Fracture Characteristics of Rock with Prefabricated Crack under Different Triaxial Stress Conditions. *Minerals* **2022**, *12*, 673. [[CrossRef](#)]
6. Zhou, X.; Peng, S.; Zhang, J.; Berto, F. Failure characteristics of coarse and fine sandstone containing two parallel fissures subjected to true triaxial stresses. *Theor. Appl. Fract. Mec.* **2021**, *112*, 102932. [[CrossRef](#)]
7. Liu, Z.; Ma, C.; Wei, X.; Xie, W. Experimental Study on the Mechanical Characteristics of Single-Fissure Sandstone Under Triaxial Extension. *Rock Mech. Rock Eng.* **2022**, *55*, 4441–4457. [[CrossRef](#)]
8. Zare, S.; Karimi-Nasab, S.; Jalalifar, H. Analysis and determination of the behavioral mechanism of rock bridges using experimental and numerical modeling of non-persistent rock joints. *Int. J. Rock. Mech. Min.* **2021**, *141*, 104714. [[CrossRef](#)]
9. Zhao, Z.; Zhou, D. Mechanical properties and failure modes of rock samples with grout-infilled flaws: A particle mechanics modeling. *J. Nat. Gas Sci. Eng.* **2016**, *34*, 702–715. [[CrossRef](#)]
10. Wang, B.; Yao, C.; Yang, J.; Jiang, S. Numerical simulation of macro-meso mechanical behaviours of sandstone containing a single open fissure under uniaxial compression. *Eur. J. Environ. Civ. Eng.* **2018**, *22*, S99–S113. [[CrossRef](#)]
11. Feng, P.; Dai, F.; Liu, Y.; Xu, N.; Zhao, T. Influence of two unparallel fissures on the mechanical behaviours of rock-like specimens subjected to uniaxial compression. *Eur. J. Environ. Civ. Eng.* **2020**, *24*, 1643–1663. [[CrossRef](#)]
12. Wang, Y.; Peng, K.; Shang, X.; Li, L.; Liu, Z.; Wu, Y.; Long, K. Experimental and numerical simulation study of crack coalescence modes and microcrack propagation law of fissured sandstone under uniaxial compression. *Theor. Appl. Fract. Mech.* **2021**, *115*, 103060. [[CrossRef](#)]
13. Chen, M.; Liu, J.; Xie, Z.; Liu, J.; Hu, X.; Li, B.; Cen, Y. Discrete Element Modeling on Mechanical Behavior of Heterogeneous Rock Containing X-Shaped Fissure under Uniaxial Compression. *Geofluids* **2020**, *2020*, 8828199. [[CrossRef](#)]
14. Wu, J.; Jing, H.; Gao, Y.; Meng, Q.; Yin, Q.; Du, Y. Effects of carbon nanotube dosage and aggregate size distribution on mechanical property and microstructure of cemented rockfill. *Cem. Concr. Compos.* **2022**, *127*, 104408. [[CrossRef](#)]
15. Wu, J.; Wong, H.S.; Yin, Q.; Ma, D. Effects of aggregate strength and mass fraction on mesoscopic fracture characteristics of cemented rockfill from gangue as recycled aggregate. *Compos. Struct.* **2023**, *311*, 116851. [[CrossRef](#)]
16. Yu, L.; Zhou, S.; Luo, X.; Niu, S.; Jiang, N. A Comparative Study of Six Hybrid Prediction Models for Uniaxial Compressive Strength of Rock Based on Swarm Intelligence Optimization Algorithms. *Front. Earth Sci.* **2022**, *10*, 930130.
17. Ren, J.; Xiao, M. Rock Macro-Meso Parameter Calibration and Optimization Based on Improved BP Algorithm and Response Surface Method in PFC 3D. *Energies* **2022**, *15*, 15176290. [[CrossRef](#)]

18. Zhang, J.; Li, P.; Yin, X.; Wang, S.; Zhu, Y. Back Analysis of Surrounding Rock Parameters in Pingdingshan Mine Based on BP Neural Network Integrated Mind Evolutionary Algorithm. *Mathematics* **2022**, *10*, 10101746. [[CrossRef](#)]
19. Zhao, G.; Yao, W.; Xing, L.; Xu, Y. Influence of Notch Geometry on the Rock Fracture Toughness Measurement Using the ISRM Suggested Semi-Circular Bend (SCB) Method. *Rock Mech. Rock Eng.* **2022**, *55*, 2239–2253. [[CrossRef](#)]
20. Yao, Y.; Zhang, Z.; Wang, W.; Li, Y.; Li, S.; Wei, C. Fuzzy Random Prediction Model of Frost Heave Characteristics of Horizontal Frozen Metro Contact Channel in Coastal Area. *Geofluids* **2022**, *2022*, 6198660.
21. Liu, S. Research on the teaching quality evaluation of physical education with intuitionistic fuzzy TOPSIS method. *J. Intell. Fuzzy Syst.* **2021**, *40*, 9227–9236. [[CrossRef](#)]
22. Ting, G.; Hu, L.; Jia, Z.; Xia, T.; Fang, C.; Li, H.; Hu, L.; Li, Y.L.H. SPXYE: An improved method for partitioning training and validation sets. *Clust. Comput.* **2019**, *22*, 3069–3078.
23. Lee, C.; Cheng, Y. Motor Fault Detection Using Wavelet Transform and Improved PSO-BP Neural Network. *Processes* **2020**, *10*, 8101322. [[CrossRef](#)]

Disclaimer/Publisher’s Note: The statements, opinions and data contained in all publications are solely those of the individual author(s) and contributor(s) and not of MDPI and/or the editor(s). MDPI and/or the editor(s) disclaim responsibility for any injury to people or property resulting from any ideas, methods, instructions or products referred to in the content.